THERMALLY DRIVEN GAS FLOW BENEATH YUCCA MOUNTAIN, NEVADA

Steven Amter
Ning Lu
Benjamin Ross

Disposal Safety Incorporated
1660 L Street NW, Suite 314
Washington, DC 20036

ABSTRACT

A coupled thermopneumatic model is developed for simulating heat transfer, rock-gas flow and carbon-14 travel time beneath Yucca Mountain, NV. The aim of this work is to understand the coupling of heat transfer and gas flow. Heat transfer in and near the potential repository region depends on several factors, including the geothermal gradient, climate, and local sources of heat such as radioactive wastes. Our numerical study shows that small temperature changes at the surface can change both the temperature field and the gas flow pattern beneath Yucca Mountain. A lateral temperature difference of 1 K is sufficient to create convection cells hundreds of meters in size. Differences in relative humidities between gas inside the mountain and air outside the mountain also significantly affect the gas flow field.

NOTATION

c	conversion factor, equal to 4.18×10^7 [erg cal^{-1}]
c_p^{gas}	specific heat of gas [cal g^{-1} K^{-1}]
c_p^{rock}	specific heat of rock [cal g^{-1} K^{-1}]
g	gravitational acceleration [cm s^{-2}]
G	geothermal gradient [K cm^{-1}]
h	freshwater head [cm]
h_a, h_v	defined by Eqs. (8)-(9) [cm]
H_v	heat of vaporization of water [cal g^{-1}]
k	permeability of rock [cm^2]
K_t	thermal conductivity of rock [cal K^{-1} cm^{-1} s^{-1}]
n	porosity [dimensionless]
P	gas pressure [Pa] [g cm^{-1} s^{-2}]
P_a	defined by $P_a=P-P_v$ [Pa] [g cm^{-1} s^{-2}]
P_{atm}	atmospheric pressure at $z=0$ [Pa] [g cm^{-1} s^{-2}]
P_o	reference pressure [Pa] [g cm^{-1} s^{-2}]
P_v	vapor pressure of water [Pa] [g cm^{-1} s^{-2}]
q	gas flux [cm s^{-1}]
R	gas constant [g cm^2 s^{-2} mol^{-1} K^{-1}]
t	time [s]
T	absolute temperature [K]
T_a	air temperature at elevation $z=0$ [K]
T_o	air temperature at elevation z_o [K]
x	horizontal coordinate [cm]
$\hat{k}$	downward-pointing unit vector
z	vertical coordinate [cm]
z_o	reference elevation near ground surface [cm]
Γ	defined by Eq. (26) [K cm^{-1}]
λ	lapse rate [K cm^{-1}]
μ	viscosity of gas [g cm^{-1} s^{-1}]
ρ	density of gas [g cm^{-3}]
ρ'	defined by Eq. (6) [dimensionless]
ρ_o	reference density of gas [g cm^{-3}]
ρ_{rock}	density of rock [g cm^{-3}]
Ω_a	molar weight of dry air [g mol^{-1}]
Ω_v	molar weight of water [g mol^{-1}]

INTRODUCTION

The U.S. Department of Energy is studying Yucca Mountain, Nevada, to determine its suitability to house a high-level nuclear waste repository. The mountain is a steep-sided linear ridge composed of alternating layers of ash-flow and bedded tuff. The potential nuclear waste repository would be located in a 500-meter thick unsaturated zone (Scott and Bonk, 1984). Gas in rock fills most of the larger-diameter pores and fractures and can move through the rock. Flow of rock gas may be important for several reasons:

- Carbon-14 released from the potential repository would migrate in the gas phase.
- Flow of water vapor out of the mountain may make an important contribution to the water balance.
- Gas convection may be a significant mechanism for removal of heat from the potential repository.

Field observations (Weeks, 1987) found seasonal airflows with speeds as high as 3.5 m/s in deep boreholes at Yucca

Mountain. These flows are believed to result from differences in gas density caused by topographic relief, seasonal temperature variation, and variation in gas composition. If a repository were built at Yucca Mountain, heat from the emplaced waste would also contribute to gas flow.

Large-scale air flows could be important to repository performance, both by influencing the distribution of carbon dioxide within the mountain and by removing water vapor from the mountain. An understanding of the effect of temperature on the gas velocity and trajectory within Yucca Mountain is necessary as input for a model of the carbon-14 distribution within the unsaturated zone (Ross, 1988), for evaluation of the net vapor flux, and for accurate heat-transfer calculations. Complete solution of this problem requires a fully coupled thermopneumatic model.

MATHEMATICAL MODEL

We have developed a model of rock-gas flow driven by temperature and humidity differences. The model is greatly simplified by assuming that the rock gas is always at 100% relative humidity. This makes it possible to model only gas-phase flow. Liquid flow is assumed sufficient to replenish evaporating water and is otherwise ignored.

Under ordinary subsurface conditions, the assumption of 100% relative humidity is quite accurate; vapor-pressure lowering is negligible because suction is much smaller than RT (RT is equivalent to 1400 bar of pressure). When temperatures reach the boiling point of water, and at locations very close to the ground surface, drying of rocks makes our model inapplicable.

The model, called TGIF, is designed in two modules: a temperature solver, which solves for the temperature field and stores calculated temperatures in the input data file for the head solver; and a head solver, which solves for the freshwater head field and gas velocities. The head solver calculates only steady-state heads, because gas pressure equilibrates very rapidly compared to repository time scales. The repository heat transfer problem is inherently transient. The calculations reported here include only steady-state heat conduction; this is a very rough approximation, and current work focuses on developing a transient heat conduction and convection model.

Gas Model

Under the assumptions that thermodynamic equilibrium exists among air, water vapor, and water and that the gas behaves as an ideal gas and is saturated with vapor, the system can be described by three equations: a volume balance (Amter and Ross, 1990), a constitutive relation, and Darcy's Law:

$$\nabla\cdot q - q\cdot\left[\left(\frac{1}{T}+\frac{1}{P_a}\frac{dP_v}{dT}\right)\nabla T-\frac{1}{P_a}\nabla P\right]=0 \qquad (1)$$

$$\rho=\frac{1}{RT}\left[P_v\Omega_v+(P-P_v)\Omega_a\right] \qquad (2)$$

$$q=-\frac{k}{\mu}(\nabla P-g\rho\hat{z}) \qquad (3)$$

If the temperature field is prescribed, solving these equations allows fields of pressure, density, and flux to be obtained. However, simulation of gas flows driven by relatively small temperature differences is hindered by the near-cancellation of the gravity and pressure-gradient forces acting on the gas. This difficulty is overcome by subtracting reference values ρ_o and P_o from the pressure and density, which allows the governing equation to be formulated in terms of the "freshwater head." With the definition of the freshwater head:

$$h=\frac{P-P_o}{g\rho_o}-z \qquad (4)$$

the Darcy flux can be written as

$$q=-\frac{g\rho_o k}{\mu}[\nabla h-\rho'\hat{z}] \qquad (5)$$

where

$$\rho'=\frac{\rho}{\rho_o}-1 \qquad (6)$$

Substitution of (4) into (1) yields

$$\nabla\cdot q - q\cdot\left[\left(\frac{1}{T}+\frac{1}{h_a}\frac{dh_v}{dT}\right)\nabla T-\frac{1}{h_a}(\hat{z}+\nabla h)\right]=0 \qquad (7)$$

where

$$h_a=P_a/g\rho_o \qquad (8)$$

$$h_v=P_v/g\rho_o \qquad (9)$$

Now we insert (5) into (7), expand, and divide by $g\rho_o$:

$$\frac{k}{\mu}\nabla^2 h-\frac{k}{\mu}\frac{\partial\rho'}{\partial z}+\nabla\left(\frac{k}{\mu}\right)\cdot\nabla h-\rho'\frac{\partial}{\partial z}\left(\frac{k}{\mu}\right)+\frac{k}{\mu h_a}(\nabla h)^2$$
$$+\frac{k}{\mu h_a}(1-\rho')\frac{\partial h}{\partial z}-\frac{k}{\mu h_a}\rho'-\frac{k}{\mu}\left(\frac{1}{T}+\frac{1}{h_a}\frac{dh_v}{dT}\right)\nabla T\cdot\nabla h$$
$$+\frac{k}{\mu}\left(\frac{1}{T}+\frac{1}{h_a}\frac{dh_v}{dT}\right)\rho'\frac{\partial T}{\partial z}=0 \qquad (10)$$

Now we expand the spatial derivatives of ρ' and μ in terms of the variables T and h_a. Using the fact that $\partial\mu/\partial P=0$ to a very good approximation, we can write

$$\nabla\left(\frac{k}{\mu}\right) = \frac{1}{\mu}\nabla k - \frac{k}{\mu^2}\frac{\partial \mu}{\partial T}\nabla T \qquad (11)$$

and

$$\frac{\partial \rho'}{\partial z} = \frac{\partial \rho'}{\partial T}\frac{\partial T}{\partial z} + \frac{\partial \rho'}{\partial h_a}\frac{\partial h_a}{\partial z} \qquad (12)$$

Inserting these expansions into (10) yields

$$\nabla^2 h - \left(\frac{\partial \rho'}{\partial T}\frac{\partial T}{\partial z} + \frac{\partial \rho'}{\partial h_a}\frac{\partial h_a}{\partial z}\right) + \frac{1}{k}\nabla k\cdot\nabla h - \frac{1}{\mu}\frac{\partial \mu}{\partial T}\nabla T\cdot\nabla h$$
$$- \frac{\rho'}{k}\frac{\partial k}{\partial z} + \frac{\rho'}{\mu}\frac{\partial \mu}{\partial T}\frac{\partial T}{\partial z} + \frac{1}{h_a}(\nabla h)^2 + \frac{1-\rho'}{h_a}\frac{\partial h}{\partial z} - \frac{\rho'}{h_a}$$
$$- \left(\frac{1}{T} + \frac{1}{h_a}\frac{dh_v}{dT}\right)\nabla T\cdot\nabla h + \left(\frac{1}{T} + \frac{1}{h_a}\frac{dh_a}{dT}\right)\rho'\frac{\partial T}{\partial z} = 0 \qquad (13)$$

From (2), (4), (6), and (8), we have

$$\rho' = \frac{g}{RT}(h_v\Omega_v + h_a\Omega_a) - 1 \qquad (14)$$

$$\frac{\partial \rho'}{\partial h_a} = \frac{g\Omega_a}{RT} \qquad (15)$$

$$\frac{\partial \rho'}{\partial T} = -\frac{g}{RT^2}(h_v\Omega_v + h_a\Omega_a) + \frac{g\Omega_v}{RT}\frac{dh_v}{dT}$$
$$= -\frac{1+\rho'}{T} + \frac{g\Omega_v}{RT}\frac{dh_v}{dT} \qquad (16)$$

$$\frac{\partial h_a}{\partial z} = \frac{\partial}{\partial z}\left[\frac{P_a}{g\rho_a} + z + h - h_v\right] = 1 + \frac{\partial h}{\partial z} - \frac{dh_v}{dT}\frac{\partial T}{\partial z} \qquad (17)$$

Substituting (15), (16), and (17) into (13) and collecting terms yields

$$\nabla^2 h - m\nabla T\cdot\nabla h + \frac{1}{h_a}(\nabla h)^2 + \left[\frac{1}{T} + g\frac{\Omega_a - \Omega_v}{RT}\frac{dh_v}{dT} + \rho'\left(\frac{1}{T} + m\right)\right]\frac{\partial T}{\partial z}$$
$$+ \left(\frac{1-\rho'}{h_a} - \frac{g\Omega_a}{RT}\right)\frac{\partial h}{\partial z} - \frac{g\Omega_a}{RT} - \frac{\rho'}{h_a} + \frac{1}{k}\nabla k\cdot(\nabla h - \rho' i) = 0 \qquad (18)$$

where

$$m = \frac{1}{\mu}\frac{d\mu}{dT} + \frac{1}{T} + \frac{1}{h_a}\frac{dh_v}{dT} \qquad (19)$$

Heat Model

Solution of the freshwater head in (18) requires that the temperature at every node in the grid be known. A temperature model is therefore needed to calculate the temperature field from specified boundary conditions.

The distribution of temperature beneath the ground surface depends upon a number of factors, including the geothermal gradient, which varies regionally and is a function of tectonic setting, topography, climatic factors affecting variation in surface temperature, and local sources of heat including radioactive rock as well as nuclear waste.

An equation for heat transfer can be written on the same basis as the gas flow equation (18), by assuming that the rock gas is always at 100% relative humidity. Because this assumption implies that moisture evaporates or precipitates wherever the gas flows through a temperature gradient, latent heat will make the largest contribution to convective heat transfer. Taking account of both sensible and latent heat gives, after some manipulation, an energy balance equation:

$$K_t\nabla^2 T - c_p^{gas}\rho q\cdot\nabla T + \frac{P}{cP_a}q\cdot\nabla P_a$$
$$+ \frac{H_v\Omega_v}{RT}q\cdot\left[\frac{P_v}{P_a}\nabla P - \frac{P}{P_a}\frac{dP_v}{dT}\nabla T\right] = c_p^{rock}\rho_{rock}(1-n)\frac{\partial T}{\partial t} \qquad (20)$$

On the left side of this equation, the first term represents conduction, the second represents sensible heat transfer, the third represents work done when the gas changes volume (to the extent not included in the second term), and the fourth represents latent heat transfer. The right side represents heating of the rock; a term representing heating of the gas in place has been dropped because $\rho << \rho_{rock}$.

As a first step, we developed a steady-state heat conduction model that accounts for topography, elevation-dependent surface temperature, the geothermal gradient, and heat generated by a radioactive waste repository and assumes that the rock has uniform and isotropic thermal conductivity. The treatment of heat transfer as conduction-dominated is unlikely to be realistic, especially when the mountain is heated by a repository. However, by limiting ourselves to steady-state simulations in which heat sources are absent or are assigned a fixed temperature (rather than a fixed heat output), we ensure that the magnitude of the thermal conductivity does not affect the results. In such cases, a conduction model can give a fair approximation to the true temperatures even when convection is an important heat-transfer mechanism.

In the future, we intend to add the other terms of Equation (20) to the heat-transfer model, so that transient problems can be simulated to calculate the temperature of the repository as a function of time.

Boundary Conditions

Boundary conditions for such coupled processes must be specified carefully. We therefore will discuss them in some detail.

Fixed pressure boundaries along the ground surface of the mountain are functions of elevation, temperature, and relative humidity. The boundary condition is derived from the ideal gas law for moist air and the laws of hydrostatics. For any fluid:

$$dP = \rho g dz \qquad (21)$$

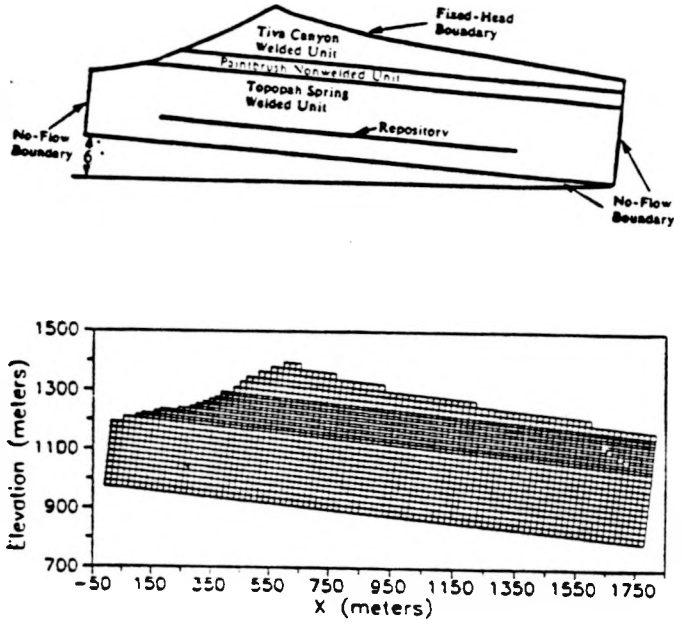

Figure 1. (a) Geometry of cross section used in the gas-flow simulation, (b) finite difference mesh.

It is assumed that temperature is linear in elevation and the mole fraction of water vapor, r, is uniform. (This implies a slight variation of relative humidity with elevation, even at uniform temperature.) The density of air is then

$$\rho = \frac{P}{R(T_a+\lambda z)}\left[r\Omega_v+(1-r)\Omega_a\right] \qquad (22)$$

where T_a is the air temperature at elevation $z=0$ and the empirical coefficient λ, the change in air temperature with altitude, is known as the "lapse rate."

Substitution of Equation (22) into (21) and integration yields

$$P = P_{atm}\left[1+\frac{\lambda z}{T_a}\right]^{\Gamma/\lambda} \qquad (23)$$

where

$$\Gamma = \frac{g}{R}\left[r\Omega_v+(1-r)\Omega_a\right] \qquad (24)$$

Unfortunately, the formula (23) becomes numerically intractable in the limit $\lambda \to 0$. This problem is overcome by using the expansion

$$(1+x)^{\alpha x} = e^{\alpha}\left[1-\frac{\alpha}{2}x+\left(\frac{\alpha}{3}+\frac{\alpha^2}{8}\right)x^2- \ \ldots\right] \qquad (25)$$

Note that inserting (25) into (23) yields the expansion in powers of λ

$$P = P_{atm}e^{\Gamma z/T_a}\left[1-\frac{\Gamma\lambda z^2}{2T_a^2}+ \ \ldots\right] \qquad (26)$$

in which the leading term corresponds to the well-known (Donn, 1975) exponential law for atmospheric pressure at constant temperature.

No-flow boundaries are assigned at the base of the simulated region (Figure 1a). This boundary corresponds to the top of the low-permeability Calico Hills nonwelded unit, which would impede downward gas flow. The boundary to the west is located in the trough of Solitario Wash, which is a natural flow divide. The third no-flow boundary is located far enough to the east to have little effect on flow near the potential repository, as shown by additional simulations not reported here. All these boundary conditions are implemented in the TGIF by setting (3) equal to zero.

The assignment of *temperature boundary* conditions in the heat model can be considered as a four-step process. The first step is to specify air temperatures along the ground surface. The second step is to use the surface temperature and an assumed geothermal gradient to assign temperatures along the bottom of the simulated region. In these two steps, it is assumed that ambient conditions apply, that is, repository heating is not yet considered. The third step is to place a boundary condition on the heat flux across the left and right sides of the simulated region. Finally, any heat sources such as radioactive decay in a repository must be included.

The temperature at the upper boundary is assumed linear in elevation. The lapse rate is usually assigned a value (Donn, 1975) of 0.65 K per 100 m.

In reality, there is no lower boundary. However, by assuming that the boundary is at a large distance and that the geothermal gradient at the boundary is uniform and vertical, the problem is greatly simplified.

With flat topography, uniform surface temperature, and no local sources of heat, isotherms would be horizontal, as shown in Figure 2a. However, this is generally not the case. Topographic relief causes isotherms to be curved near the earth's surface. An exception to this rule would occur if the lapse rate were equal to the geothermal gradient. This unphysical case is illustrated in Figure 2b.

Curvature of isotherms resulting from small-scale relief damps out rapidly with depth, usually within a few meters or tens of meters, as illustrated in Figure 2c. However, large scale variations in topography can cause curvature of isotherms to extend to considerable depths, as shown in Figure 2d. When simulating such a case, it is important that the lower boundary be placed far enough below the surface, or other sources of heat such as a repository, to make the fixed-temperature lower boundary a reasonable approximation to a boundary at infinity.

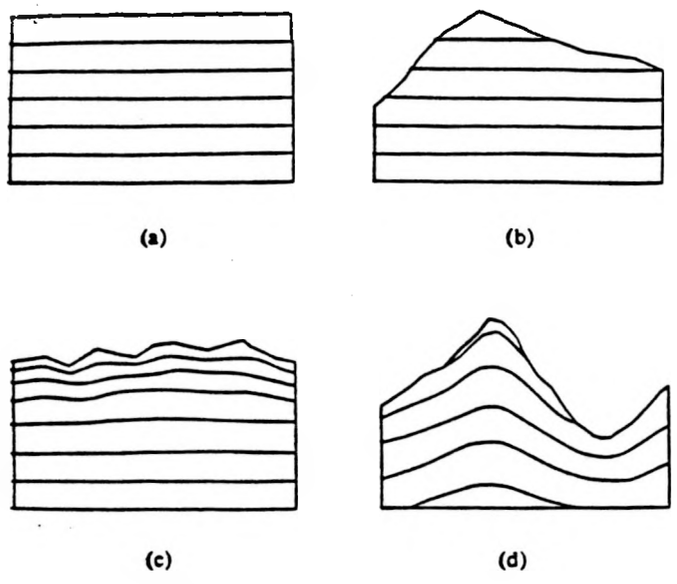

Figure 2. Schematic temperature contours showing the relationship among the geothermal gradient, lapse rate, and topography: (a) flat topography and uniform surface temperature; (b) irregular topography and lapse rate equal to the geothermal gradient; (c) geothermal gradient exceeding the lapse rate with small topographic relief; (d) geothermal gradient exceeding the lapse rate with large topographic relief.

To improve the calculation of the temperature field in such cases, the finite difference grid can be extended downward. This option extends the grid in the temperature model, but not in the flow model. It adds ten rows of blocks with vertical spacing that increases approximately exponentially. Temperatures along the lower boundary are calculated from

$$T = T_s + G[z - z_s] \qquad (27)$$

where z_s is a specified elevation on the ground surface and T_s is the temperature at that elevation. The lower boundary condition is the same whether or not the extension option is used.

The boundary condition along the left and right sides require the heat flux to be vertical. When the grid is not tilted, this condition can easily be met by using the method of reflection to specify no flow. However, a modification of reflection is necessary to constrain the flux to be vertical when the side boundaries are tilted from the vertical.

The usual way to apply the technique of reflection is to set the node on the boundary equal to an interior node. If the grid boundary is tilted from vertical, simple reflection will result in a tilted no-flow boundary. Because the system has an imposed flow of heat upward from the bottom, this will have the effect of imposing a horizontal heat flux at the boundaries. For there to be a horizontal component of heat flux, there must also be a horizontal component of the temperature gradient.

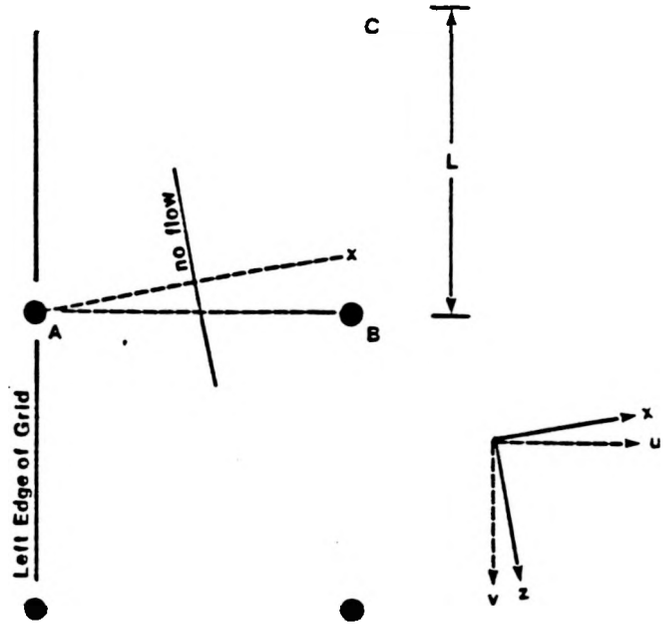

Figure 3. Illustration of vertical flux boundary condition for a tilted grid.

Artificially imposed horizontal temperature gradients, even if small, are very undesirable because horizontal temperature differences drive convection cells in the gas flow model.

To force the heat flux at the boundary to be exactly vertical, the reflection technique must be modified so that the reflection occurs across a vertical plane. The temperature of the node on the grid boundary is set to the temperature at a point that is found by extending a horizontal line from the node on the boundary to the line of the adjacent column of nodes. The temperature at this point can be found by linear interpolation between the adjacent nodes.

Figure 3 illustrates how the technique is applied at a left-side boundary tilted clockwise. The temperature at point A is set equal to the temperature at point x, which is found by linear interpolation of temperature between B and C. Note that a discontinuous no-flow boundary results when the condition is applied along a line of nodes .

Heat sources due to radioactive decay are simulated in the conduction-only model by assigning fixed temperatures to nodes located along the repository. These temperatures may represent cooldown at certain times in the repository's history. Mathematically, the repository is treated as a fixed-temperature boundary, although the "boundary" is located in the interior of the simulation region. In the future conduction-convection model, a source term with a specified rate of heat generation will be added to Equation (20) at the repository nodes.

The finite difference method is used to calculate both the temperature field and the gas flow field. To speed convergence, Gauss-Seidel iteration and successive overrelaxation are used. All calculations were made by 80286- and i486-based microcomputers, using no more than 640 kbyte of memory.

SIMULATION RESULTS

Figure 1a shows a two-dimensional vertical cross section that cuts across the south portion of Yucca Mountain. The mountain contains a number of hydrostratigraphic subdivisions of the Paintbrush Tuff Formation. Most of the mountain is composed of densely fractured welded tuff, which we assume has a relatively high permeability of 10^{-7} cm^2. The most prominent hydrostratigraphic feature is a thin nonwelded tuff layer which includes all or part of several stratigraphic subdivisions of the Paintbrush Tuff (Scott and Bonk, 1984). This Paintbrush nonwelded unit is sparsely fractured and thus is thought to have a lower permeability.

Figure 1b illustrates the numerical discretization of the cross section. Smaller spacing is used in the nonwelded tuff region to provide better resolution of the path-line refraction that occurs at the permeability interface.

Lapse rate

The effect of surface temperature change on temperature field is illustrated in Figure 4. Figure 4a is the temperature field with a lapse rate of 0.65 K/100 m applied at the atmospheric boundary, while Figure 4b shows the temperature field with the lapse rate set to a geothermal gradient of 2 K/100 m. In both cases, the relative humidity of the atmosphere is 20%. In Figure 4a, isotherms are curved near the surface because the lapse rate is not equal to the geothermal gradient. The curvature damps out as the depth increases. With the lapse rate equal to the geothermal gradient, equally spaced horizontal isotherms are obtained (Figure 4b).

The corresponding gas flow fields are shown in Figures 5a and b. Since a high permeability contrast (1000×) between welded and nonwelded tuffs is used, gas flow forms two systems; one above the nonwelded tuff layer, the other below the nonwelded tuff layer. A strong convection cell is formed in the case of lapse rate equal to 0.65 K/100 m, but no convection cell is found when the lapse rate is equal to the geothermal gradient (The apparent flow around the right end of the repository shown in Figure 5b is much slower than that shown in Figure 5a.).

Relative humidity

To examine the effect of atmospheric relative humidity on the gas flow, two relative humidity values of 20% and 100% were compared. The gas flow field with 20% relative humidity is shown in Figure 5. Gas flow velocities obtained with 100% relative humidity in the atmosphere are as small as the computer's precision permits. No particle originating inside the mountain will be released to the atmosphere. The numerical result shows that the model predicts no significant flow at 100% relative humidity. This is expected, because in the absence of a relative humidity contrast, with a uniform temperature gradient, gas density varies directly with elevation and there is no driving force. Thus gas reaches its static equilibrium under uniform temperature gradient.

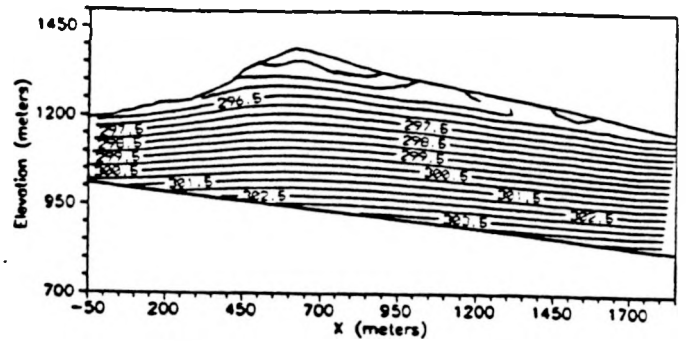

Figure 4a. Temperature field with a lapse rate of 0.65 K/100 m applied at the atmospheric boundary.

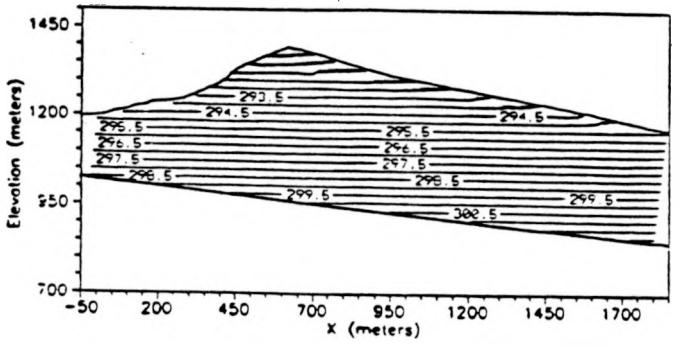

Figure 4b. Temperature field with the lapse rate equal to the geothermal gradient.

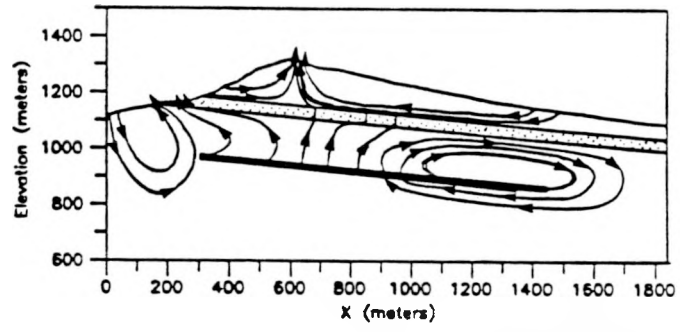

Figure 5a. Gas flow field with a lapse rate of 0.65 K/100 m.

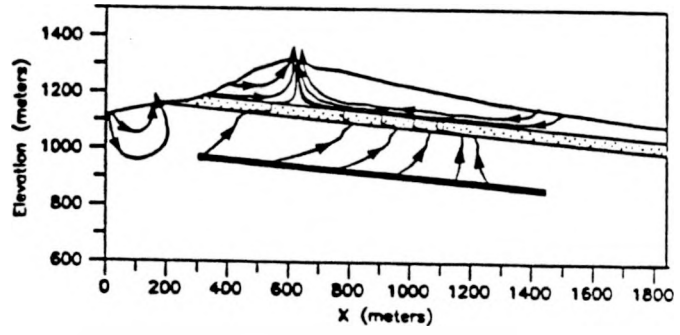

Figure 5b. Gas flow field with the lapse rate equal to the geothermal gradient.

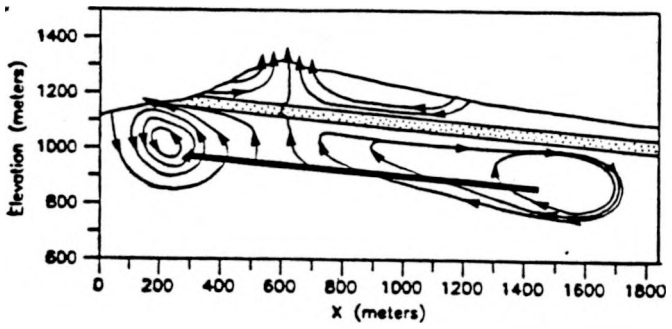

Figure 6. Gas flow field with the repository at 330 K; conditions otherwise identical to Figure 5a.

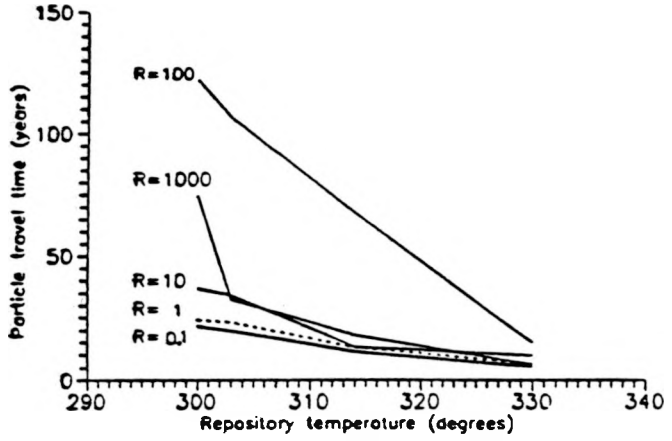

Figure 7. The minimum particle travel time from the potential repository as a function of temperature at the potential repository. (R is the ratio of permeability between welded and nonwelded tuffs.)

The calculated gas velocities around the right end of the potential repository (Figures 5a and b) are much smaller than those near the mountain surface. This may reflect that the area is surrounded by two no-flow boundaries (left and bottom), and one relatively impermeable layer (nonwelded tuff) and is far away from the ground surface so that there is little effect due to the relative humidity difference.

Repository temperature

Figures 6 and 7 show how temperature changes at the potential repository affect gas flow field and the travel time from the potential repository to the ground surface. When the temperature reaches 330 K at the repository, strong convection cells are formed around the both ends of the repository. Study (Lu, et al, 1991) showed that the gas flow pattern changes as the potential repository cools. Simulations show that, in general, particle travel time decreases as the potential repository temperature increases. For instance, when the permeability contrast is 100, unretarded particle travel time is about 125 years when the potential repository temperature is 300 K (corresponding to the ambient condition), while it is only 20 years when the potential repository is heated to 330 K.

CONCLUSIONS

This study uses a preliminary heat transfer model to examine how temperature changes at the ground surface, the potential repository, and the model boundary affect the temperature and gas flow fields. Simulations demonstrate that our gas flow model is very sensitive to the temperature variation on the boundaries and that a small temperature change at the surface will change both the temperature field (Figure 4) and gas flow pattern (Figure 5) beneath Yucca Mountain. A lateral temperature difference of 1 K is sufficient to create convection cells hundreds of meters in size. The temperature field is sensitive to seemingly unimportant changes in the boundary conditions. Relative humidity differences between gas inside the mountain and air outside the mountain play an important role in gas flow in Yucca Mountain.

As a first step, we treated temperature as an independent variable and heat transfer as conduction-dominated. Future work will be directed to building a fully coupled model in which temperature is treated as a dependent variable and convection of both sensible and latent heat is considered. In addition, heat released from the potential repository will be simulated as a function of time.

ACKNOWLEDGMENTS

This work was supported by Sandia National Laboratories under the auspices of the U.S. Department of Energy, Office of Civilian Radioactive Waste Management, Yucca Mountain Project, under Contract DE-AC04-76DP00789.

REFERENCES

Amter, S. and B. Ross, "Simulation of Gas Flow Beneath Yucca Mountain, Nevada, with a Model Based on Freshwater Head," *Proceedings of the Symposium on Waste Management*, edited by R.G. Post, Tucson AZ, vol. 2, pp. 915-925, 1990.

Donn, W.L., *Meteorology*, 4th edition, McGraw Hill, New York, 1975.

Lu, N., S. Amter and B. Ross, "Effect of A Low-Permeability Layer on Calculated Gas Flow at Yucca Mountain," *Proceedings of the 2nd Intl. Conference on High Level Waste Management*, vol. 1, pp. 853-860, 1991.

Ross, B., "Gas-Phase Transport of Carbon-14 Released From Nuclear Waste into the Unsaturated Zone," *Scientific Basis for Nuclear Waste Management XI*, edited by M.J. Apted and R.E. Westerman, Materials Research Society, Pittsburgh, pp. 273-284, 1988.

Scott, R.B., and J. Bonk, "Preliminary Geologic Map of Yucca Mountain, Nye County, Nevada, with Geologic Sections," U.S. Geological Survey Open-File Report 84-494, Denver, CO, 1984.

Weeks, E.P., "Effect of Topography on Gas Flow in Unsaturated Fractured Rock--Concepts and Observations," *Flow and Transport Through Unsaturated Fractured Rock*, edited by D.D. Evans and T.J. Nicholson, Geophysical Monograph 42, American Geophysical Union, pp. 165-170, 1987.